

Subsurface defect of the SiO_x film imaged by atomic force acoustic microscopy

He Cunfu*, Zhang Gaimei, Wu Bin, Wu Zaiqi

College of Mechanical Engineering & Applied Electronics Technology, Beijing University of Technology, Beijing 100124, China

ARTICLE INFO

Available online 24 April 2010

Keywords:

SiO_x film
Acoustic amplitude image
Atomic force acoustic microscopy
Local elasticity
Subsurface defect

ABSTRACT

Atomic force acoustic microscopy (AFAM) has been developed in order to evaluate mechanical properties of the materials at nano-scale. The SiO_x films on the silicon wafer and glass slide were prepared by plasma enhanced chemical vapor deposition (PECVD) and their properties were characterized by atomic force acoustic microscopy (AFAM). The images of the amplitude of the vibrating cantilever were visualized for the sample vibrating at the ultrasonic frequency and the characteristics of the images were also discussed at the different excitation frequencies. The results showed that the acoustic amplitude images can provide information about the local elasticity and the subsurface defects of the materials qualitatively.

© 2010 Published by Elsevier Ltd.

1. Introduction

With the development of micro-electromechanical devices and food packaging barrier materials, the SiO_x films have received considerable attention recently. Due to inappropriate technologies, SiO_x barrier films, deposited on the substrates by plasma enhanced chemical vapor deposition (PECVD) [1,2], are sometimes with subsurface defects. These defects would deteriorate the barrier and mechanical properties of the materials. So, effective and reliable nondestructive tests are needed for quality assurance purposes of the process. To predict the performance of the barrier material and to evaluate its reliability at nano-scale, the novel inspect method with high lateral resolution is needed. Atomic force microscopy (AFM) [3–5] and scanning electron microscopy (SEM) [6,7] can reveal the surface characteristic of SiO_x coatings described as granular. But the subsurface defect of the SiO_x films cannot be revealed. Although the subsurface defects can be examined by cross-sectional high-resolution transmission electron microscopy (TEM), it has difficulties associated with sample preparation and defect identification [7,8]. AFM can measure the three dimensional topography as well as physical properties of a surface with a sharpened probe. When an ultrasonic wave is coupled into the sample, such that the sample surface vibrates at ultrasonic frequencies, the sensor tip and the cantilever are also forced to vibrate around their equilibrium position. If only very small vibration amplitudes of the cantilever around its equilibrium position are excited, the tip-sample force can be expanded linearly, and it can be represented by a linear spring with a spring constant [9]. The quantity that is used to determine Young's modulus of sample surface is the tip-sample vertical contact stiffness

in atomic force acoustic microscopy (AFAM) system. Based on the theory, the mechanical properties can be characterized by AFAM at nano-scale.

AFAM is a dynamical technique [9–12], where the cantilever or the sample surface is vibrated at ultrasonic frequencies while a sample surface is scanned with the sensor tip contacting the sample. As a consequence, the amplitude of the cantilever vibration as well as the shift of the cantilever resonance frequencies contain information about local tip-sample contact stiffness and can be used as imaging quantities [13]. The AFAM technique has been demonstrated to be a powerful tool for the investigation of the local elastic properties of sample surface [9,11,12,14]. Moreover, in the case of a thin film deposited over a substrate, AFAM measurements are less affected by mechanical properties of the substrate itself [15,16]. In this study, we have developed the atomic force acoustic microscope (AFAM) system based on the atomic force microscope and researched the SiO_x film on the silicon and glass slide substrates so as to analyze local mechanical properties of the film. It is interesting that the subsurface defects were shown in the acoustic amplitude images.

2. Experimental investigation

2.1. Sample preparation

The single crystal silicon <111> wafers and glass slides as the substrates were cleaned sequentially in an ultrasonic bath using ethanol, acetone, and deionized water before they were mounted on the sample holder. Hexamethyldisiloxane (HMDSO) in mixture with oxygen (O₂) was used as deposition gases. The SiO_x films were deposited by plasma enhanced chemical vapor deposition (PECVD) through glow discharge. The conditions of making the sample are that the background pressure was 4.1 Pa, oxygen flow

* Correspondence to. No.100, Pingleyuan, Chaoyang District, Beijing, PR China.
Tel.: +86 1067391938; fax: +86 1067391617.

E-mail address: hecunfu@bjut.edu.cn (H. Cunfu).

rate was 21 sccm (standard cubic centimeter per minute), monomer flow rate was 10.5 sccm, and input power (200 W) was kept for 20 min during the deposition.

2.2. Experimental set-up

A modified commercial atomic force microscope (CSPM 5000, Ben Yuan, China) is used to image the sample surface and to control the static cantilever forces before the tip contacts the sample (Fig. 1). The constituent components include (1) an AFM instrument, (2) a function generator and piezoelectric transducer to excite the cantilever resonances, (3) a lock-in amplifier for frequency selective signal detection, and (4) a computer for instrument control and data acquisition.

An external function generator (AFG3021, Tektronix, USA) provides a stable sinusoidal excitation, which is applied to a piezoelectric transducer coupled to the back side of the sample. The transducer with a center frequency of 1 MHz in thickness vibration is used. It emits longitudinal acoustic waves into the sample, which causes out-of-plane vibration of the sample surface. These surface vibrations are transmitted into the cantilever via the sensor tip. The cantilever vibrations are measured by the photodiode detector with sufficient bandwidth of the AFM, and from which the signal is connected to the input of a lock-in amplifier (Model 7280 DSP, Signal Recovery, USA). The sync signal from the function generator provides the reference signal for the lock-in amplifier. While the sample surface is scanned by the probe and excited at a fixed excitation frequency, the amplitude of the cantilever is modulated by the lock-in amplifier and fed into an auxiliary input channel of the AFM in order to image. Figs. 1 and 2 show the block diagram and photograph of the AFAM system.

2.3. Getting the image

To image the acoustic amplitude of the cantilever, the original up-down signal from the photodiode detector is connected to the signal channel of lock-in amplifier and the excitation signal from the function generator is connected to the reference channel of lock-in amplifier. Consequently, the amplitude of the cantilever was modulated. When the sample was scanned, the acoustic amplitude images were also obtained using the additional channel of AFM except for the topography images. We can obtain the acoustic amplitude images at different excitation frequency



Fig. 2. Photograph of AFAM system.

for the same area of the sample, which can reflect the local contact stiffness, local elasticity of the sample, and the subsurface defect.

3. The results and discussion

3.1. The acoustic amplitude images

Fig. 3 showed the topography image (a) and the acoustic amplitude images (b) for the same surface area ($12 \times 12 \mu\text{m}^2$) of SiO_x film on the silicon substrate excited at the 100 kHz frequency. In Fig. 3(a), dark regions indicated lower morphology and brighter regions indicated higher one, and no more information can be shown. Fig. 3(b) shows the acoustic amplitude images, which are different from the Fig. 3(a). The resulting image contains the relative amplitude of the cantilever vibration at the excitation frequency for each position on the sample. As the topography image, the amplitude is higher in brighter regions and smaller in darker regions. We can find that the images in Fig. 3(a) and (b) are inverse in brightness for almost all areas such as in circled region. It can be deduced that the sample is without subsurface defects.

3.2. The subsurface defect in acoustic amplitude images

Fig. 4(a) and (b) showed the topography and acoustic amplitude images of the same $3.59 \mu\text{m} \times 3.59 \mu\text{m}$ area when the SiO_x film on the glass substrate is excited at the 250 kHz frequency and with 1 V amplitude. We can find that in the two images of the same areas the contrast is accordant in brightness, such as in circled ellipse regions. It is interesting that we can observe the subsurface defect in acoustic amplitude images in Fig. 4(b). From Fig. 4(b), we can find a dark line on the left side corresponding to line defects existing on the subsurface, which does not appear in topography images in Fig. 4(a). The dark line shows that the amplitude of the cantilever is much smaller than other areas due to the decreasing of the elastic modulus.

Figs. 5 and 4 correspond to the same area of the sample. Fig. 5(a) and (b) showed the topography and acoustic amplitude images when the sample was excited at the 50 kHz frequency and with 1 V amplitude. From Figs. 4(a) and 5(a), we can see that the topographies are almost the same except a little moving up due to the drift during the scanning. But the acoustic amplitude images varied with the excitation frequency, seen in Figs. 4(b) and 5(b).

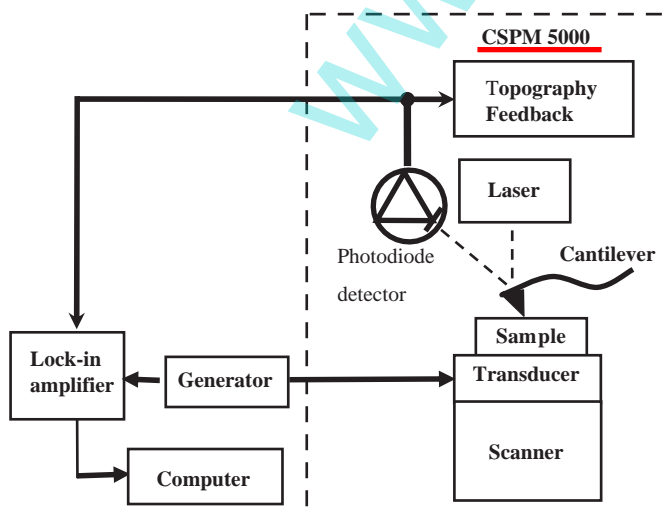


Fig. 1. Block diagram of AFAM system.

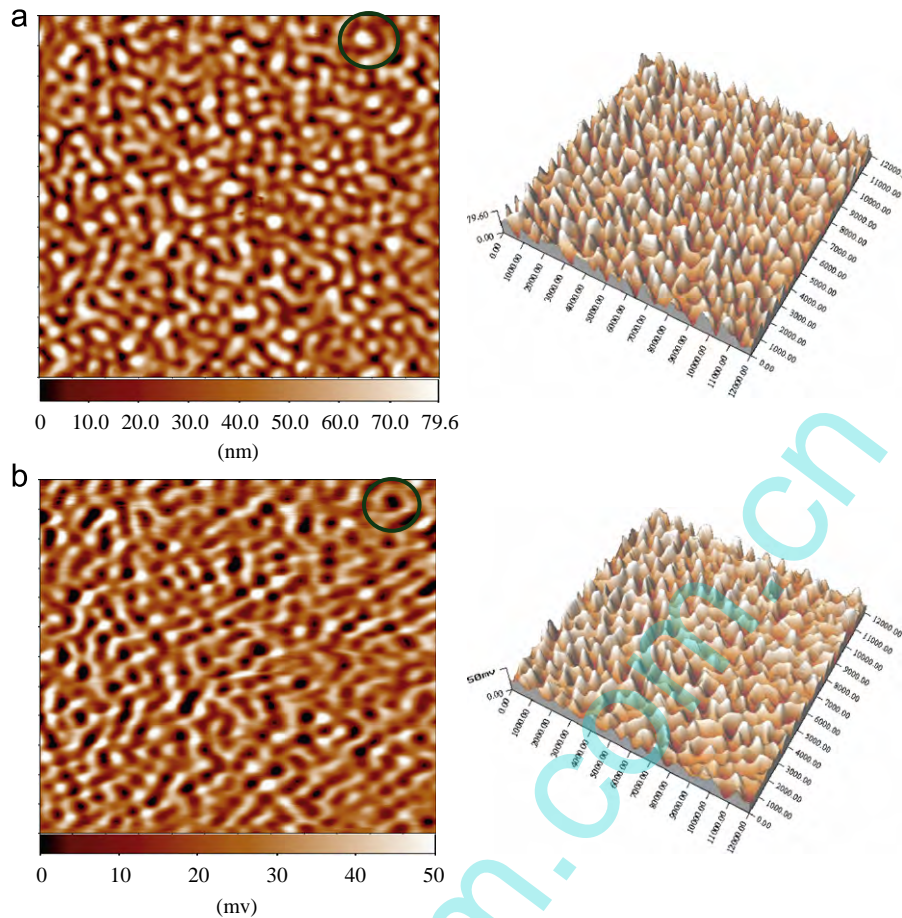


Fig. 3. Topography (a) and acoustic amplitude (b) images of SiO_x film on the silicon excited at the 100 kHz.

3.3. Analysis and discussion

3.3.1. Forced flexural vibrations of the cantilever

If the vibration amplitudes of the tip and sample are kept sufficiently small, the tip-sample forces can be approximated by linear vertical spring dashpot systems. If considering that the tip is located at the end of the cantilever, the cantilever angle is assumed to be zero, and the damping constants is neglected because the contact stiffness is the most important factor determining the Young's modulus of the sample surface [16], a simplified model is shown in Fig. 6 [9]. The characteristic equation of the simplified system shown in Fig. 6 as follows:

$$\frac{k^*}{k_c} (\sin k_n L \cos k_n L - \sin k_n L \cosh k_n L) = \frac{(k_n L)^3}{3} (1 + \cos k_n L \cosh k_n L) \quad (1)$$

where k_c is the spring constant of the cantilever, k_n is the wave numbers of the cantilever; k^* is the tip-sample contact stiffness; L is the total length of the cantilever.

The vertical contact force can be estimated using the Hertz model for a spherical indenter with radius R contacting a flat surface. According to the Hertz model we can obtain:

$$k^* = \sqrt[3]{6E^*R F_0} \quad (2)$$

where E^* is the effective Yong's modulus of the tip-sample contact; F_0 is the normal force acting on the sensors tip.

Furthermore, we also have:

$$(E^*)^{-1} = \frac{1 - \nu_t^2}{E_t} + \frac{1 - \nu_s^2}{E_s} \quad (3)$$

where E_t , E_s and ν_t , ν_s are the Yong's modulus and Poisson rates of the tip and the sample, respectively. So, we can measure k^* and deduce elastic prosperities of the samples if the material parameters (E_t, ν_t) of tip are given. k^* will increase with the increasing elastic modulus of the sample surface.

3.3.2. Contact resonance spectra analysis

Suppose that the amplitude of excitation signal is y_0 ; the deflection of the cantilever is described by following equation [9]:

$$y = y_0 \left((\cos k_n L - \cosh k_n L) - \frac{\cos k_n L + \cosh k_n L}{\sin k_n L + \sinh k_n L} (\sin k_n L - \sinh k_n L) \right) \quad (4)$$

The AFM cantilever is made of silicon with the dimensions of $160 \times 41 \times 4.6 \mu\text{m}^3$ and a stiffness (k_c) of about 40 N/m. The Young's modulus E_t of silicon is $1.69 \times 10^{11} \text{ N/m}^2$ and the mass density is 2330 kg/m^3 . With Eq. (4), using these parameters for different contact stiffness (k^* is 40.56 and 40.64 N/m) we can calculate the contact resonance spectra such as Fig. 7. It can be found that surfaces with higher elastic modulus generate contact resonance curves with increased center frequency and higher amplitude. When the excitation frequency is below the frequency responding to the cross point of the two curves, the amplitude of the contact resonance spectra on the lower k^* areas is higher than one on the higher k^* areas. When the excitation frequency is above the frequency responding to the cross point of the two curves, the amplitude of the contact resonance spectra on the higher k^* areas is higher than one on the lower k^* areas.

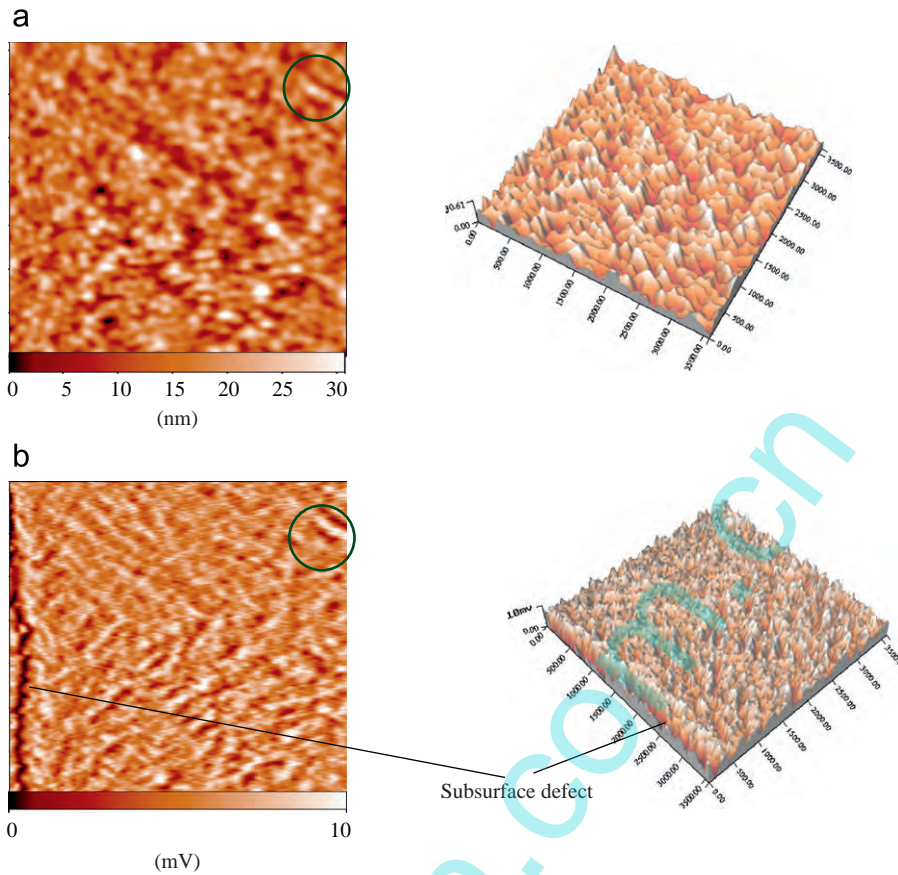


Fig. 4. Topography (a) and acoustic amplitude (b) images of SiO_x film on glass slide excited at the 250 kHz.

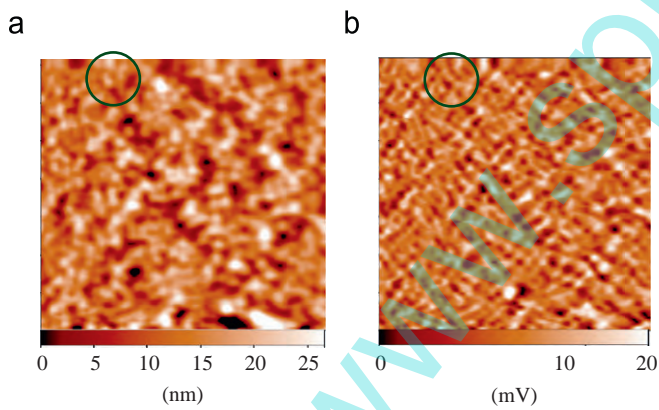


Fig. 5. Topography (a) and acoustic amplitude (b) images of SiO_x film on glass slide excited at the 50 kHz.

3.3.3. Acoustic amplitude images analysis

In AFAM, the acoustic wave would transmit and result in displacement field in the sample when the piezoelectric transducer is vibrated under AC voltage. While in the case of acoustic amplitude imaging, the amplitude contrasts reflect the responses of SiO_x film to the local elastic displacement fields in the sample, which is closely relevant to the local contact stiffness between the tip and the sample surface during scanning. Regions with higher elastic modulus, called as stiff regions, generate contact resonance curves with increased center frequency and higher amplitude than regions with lower elastic modulus, called as soft regions [16,17]. When the tip scans the higher regions of the topography image, the tip-sample repulsion is bigger. Equivalently the contact stiffness is

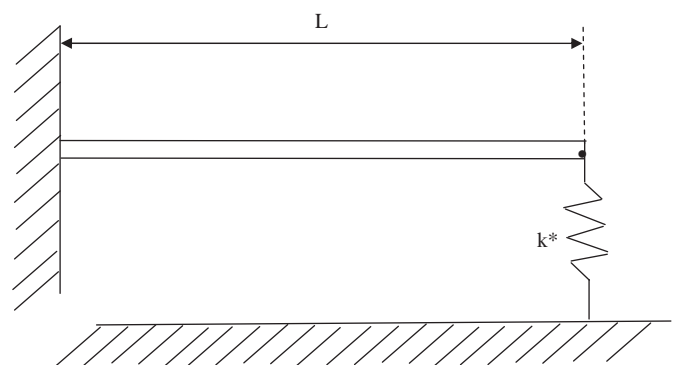


Fig. 6. Flexural beam model for the AFM cantilever with sensor tip.

bigger than lower regions of the topography. If the excitation frequency is near the contact response frequency of the stiff regions (higher regions of topography image), in which the acoustic amplitude of the cantilever is higher, so the contrast of the two images are consistent in brightness [17], as Fig. 4 (a) the topography and (b) acoustic amplitude images in ellipse regions. When the excitation frequency is near the contact response frequency of the soft regions (lower regions of topography image), in which the acoustic amplitude of the cantilever is higher than the stiff regions, the contrast in brightness of the two images is inverse, as the images in Figs. 3 and 5.

3.3.4. Subsurface defects analysis

If there are subsurface defects areas, the tip-sample contact stiffness is smaller and the center frequency of contact response

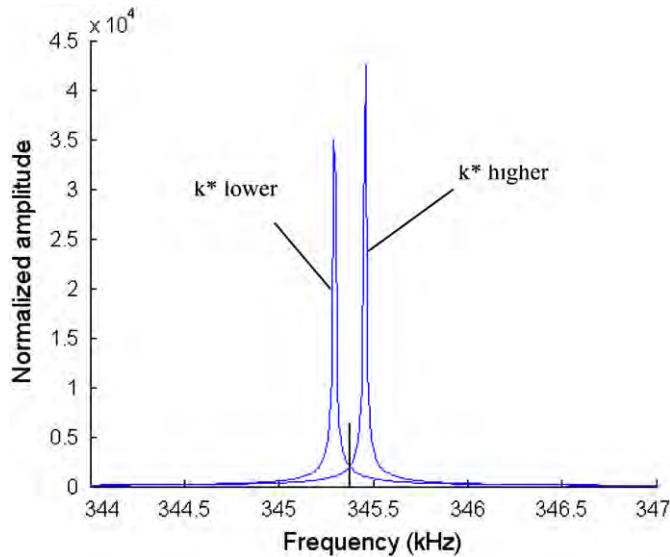


Fig. 7. Calculating contact resonance spectra.

frequency is lower. If the excitation frequency is far from the contact response frequency, the acoustic amplitude of the cantilever is very low. So, the contrast of the amplitude image depends on not only the topography but also the presence of subsurface defect. Fig. 3 showed the images of sample without the subsurface defect, the contrast in brightness is inverse between the topography and acoustic amplitude images for almost all areas. Because the decrease in amplitude (or increasing) induced by subsurface defect is more remarkable than by the topography, the contrast of brightness is not totally inverse (or consistent) in all areas between the topography and acoustic amplitude images, shown in Figs. 4(b) and 5(b). Maybe the glass slide is not clear enough, and the subsurface defect is appearing.

4. Conclusions

In summary, SiO_x film was characterized by atomic force acoustic microscopy. The results showed that the acoustic amplitude image was relevant to the contact stiffness and local elastic properties induced by topography and subsurface defect. The acoustic amplitude images can be obtained when the sample was excited at different frequencies. We can find the subsurface defect in acoustic amplitude image when the sample is excited at the suitable frequency. It is proved the atomic force acoustic microscopy is a useful method for mapping subsurface defects.

Acknowledgement

This work was supported by the National Natural Science Foundation (No. 50775005) of China. We thank D C Hurley, National Institute of Standards & Technology of USA, and Wu Junhan, engineer of Benyuan company, for the help in building the AFAM system.

References

- [1] Walker M, Meermann TF, Schneider J, Bazzoun K, Feichtinger J, Schulz A, et al. Investigations of plasma polymerized barrier films on polymeric materials. *Surf Coat Technol* 2005;200:947–52.
- [2] Zhou Mei-Li, Fu Ya-Bo, Chen Qiang, Ge Yuan-Jing. Deposition of SiO_x barrier films by O_2/TMDSO RF-PECVD. *Chin Phys* 2007;16:1101–4.
- [3] Garcia-Ayuso G, Vazquez L, Martinez-Duart A. AFM morphological surface characterization of transparent gas diffusion barrier coating on plastic films. *Surf Coat Technol* 1996;80:203–6.
- [4] Barker CP, Kochem KH, Revell KM. Atomic force microscopy and permeability study of stretching-induced gas barrier loss of AlO_x layers. *Thin Solid Films* 1995;259:46–52.
- [5] Mallik RR, Butler Jr. T, Kulnis Jr. WJ, Confer TS, Henriksen PN. Characterization of ultrathin sputtered SiO_x films on alumina by inelastic electron tunneling spectroscopy and atomic force microscopy. *J Vac Sci Technol A* 1992;10:2412–8.
- [6] Thyen R, Weber A, Klages CP. Plasma-enhanced chemical-vapour-deposition of thin films by corona discharge at atmospheric pressure. *Surf Coat Technol* 1997;97:426–34.
- [7] Philips RW, Markantes T, LeGallee C. In: SVC 36th annual technical conference proceedings 1993; p. 293.
- [8] Henry BM, Roberts AP, Grovenor CRM, Sutton AP, Briggs GAD, Tsukahara Y, et al. In: SVC 41st annual technical conference proceedings 1998; p. 434.
- [9] Rabe U, Janser J, Arnold W. Vibrations of free and surface-coupled atomic force microscope cantilevers: theory and experiment. *Rev Sci Instrum* 1996;67:3281–93.
- [10] Passeri D, Rossi M, Alippi A, Bettucci A, Terranova ML, Tamburri E, et al. Characterization of epoxy/single-walled carbon nanotubes composite samples via atomic force acoustic microscopy. *Physica E* 2008;40:2419–24.
- [11] Rabe U, Amelio S, Kester E, Scherer V, Hirsekorn S, Arnold W. Quantitative determination of contact stiffness using atomic force acoustic microscopy. *Ultrasonics* 2000;38:430–7.
- [12] Hurley DC, Shen K, Jennett NM, Turner JA. Atomic force acoustic microscopy methods to determine thin-film elastic properties. *J Appl Phys* 2003;94:2347–54.
- [13] Rabe U, Amelio S, Kopycinska M, Hirsekorn S, Kempf M, Goken M, et al. Imaging and measurement of local mechanical material properties by atomic force acoustic microscopy. *Surf Interface Anal* 2002;33:65–70.
- [14] Passeri D, Bettucci A, Germano M, Rossi M, Alippi A. Effect of tip geometry on local indentation modulus measurement via atomic force acoustic microscopy technique. *Rev Sci Instrum* 2005;76:093904.
- [15] Kopycinska-Müller M, Geiss RH, Müller J, Hurley DC. Elastic-property measurements of ultrathin films using atomic force acoustic microscopy. *Nanotechnology* 2005;16:703–9.
- [16] Amelio S, Goldade AV, Rabe U, Scherer V, Bhushan B, Arnold W. Measurement of elastic properties of ultrathin diamond-like carbon coatings using atomic force acoustic microscopy. *Thin Solid Films* 2001;392:75–84.
- [17] Zeng JT, Zhao KY, Zeng HR, Song HZ, Zheng LY, Li GR, et al. Subsurface defect of amorphous carbon film imaged by near acoustic microscopy. *Appl Phys A* 2008;91:261–5.